Electronic Supplementary Material (ESI) for Journal of Materials Chemistry A.

Supporting Information

Construction of MXene functionalized wood-based hydrogels using $ZnCl_2$ aqueous solution for flexible electronics

Zhongguo Wang, Xiong-Fei Zhang*, Lian Shu and Jianfeng Yao*

Jiangsu Co-Innovation Centre of Efficient Processing and Utilization of Forest Resources, College of Chemical Engineering, Nanjing Forestry University, Nanjing 210037, China

*Corresponding authors.

E-mail: zxf1990@njfu.edu.cn; jfyao@njfu.edu.cn

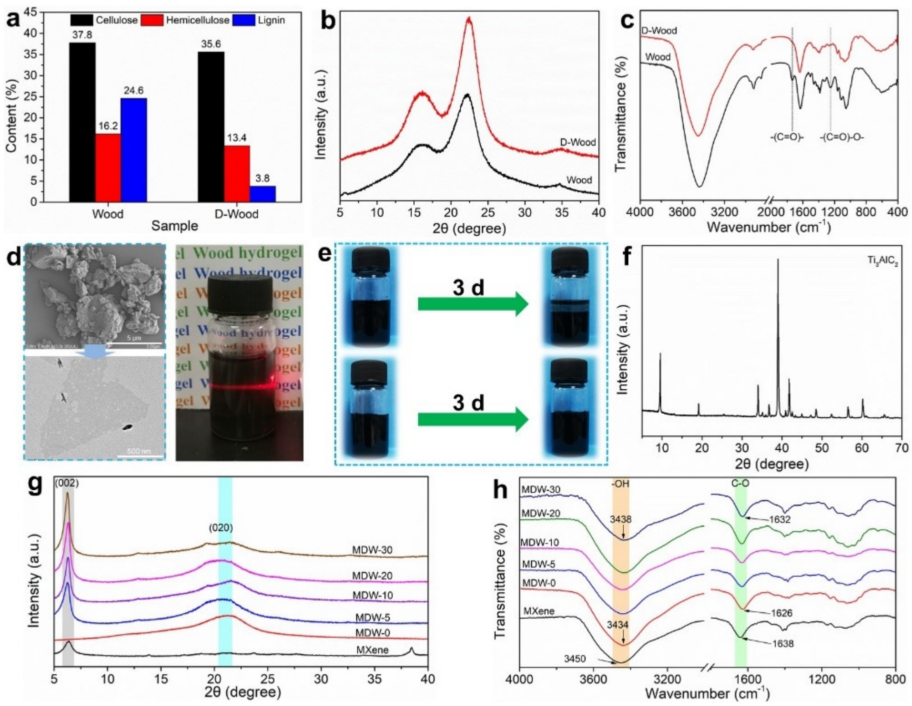

Fig. S1 (a) The content of cellulose, hemicellulose and lignin. (b) XRD patterns and (c) FT-IR spectra of Wood and D-Wood. (d) SEM and TEM images of the Ti_2AlC_3 and MXene, and the suspension of MXene with a strong Tyndall effect. (e) Photos of MXene solution placed for 3 day in aqueous solution (up) and $ZnCl_2$ solution (down). (f) XRD pattern of Ti_2AlC_3. (g) XRD patterns and (h) FT-IR spectra of composite hydrogels (freeze-dried samples).

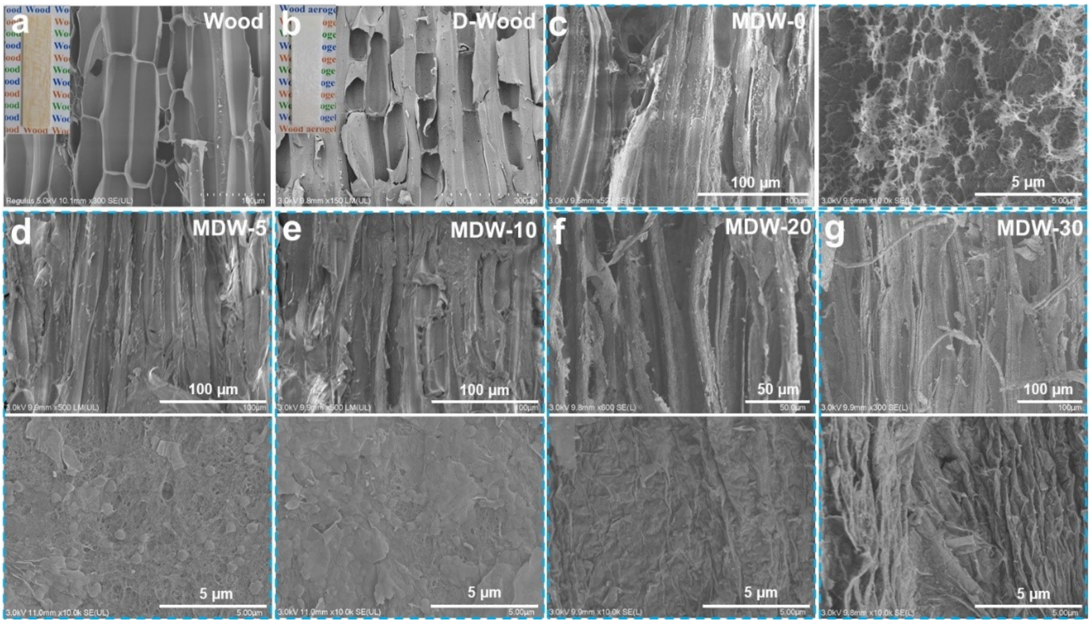

Fig. S2 SEM images of the (a) Wood, (b) D-Wood and (c-g) composite hydrogels.

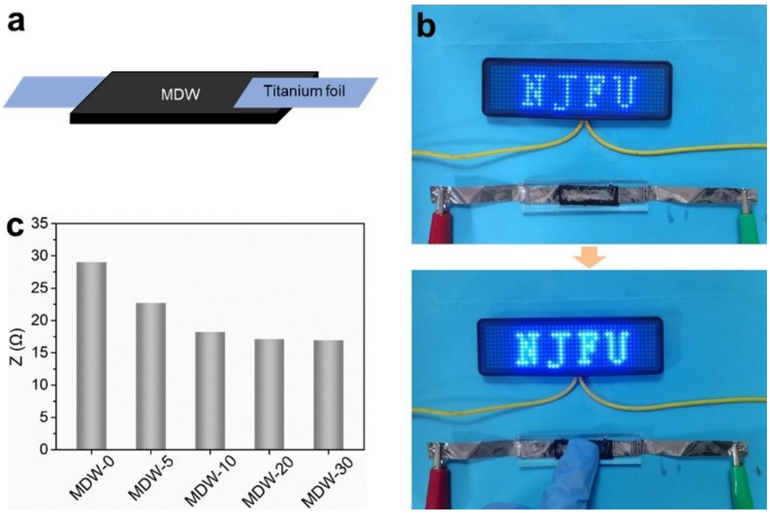

Fig. S3 (a) Assembly diagram of sensor (In our experimental, such sensor was wrapped with polydimethylsiloxane film to protect skin). (b) Digital images of the luminance variations of LED lamp responding to different status. (c) The resistance of MDW at room temperature.

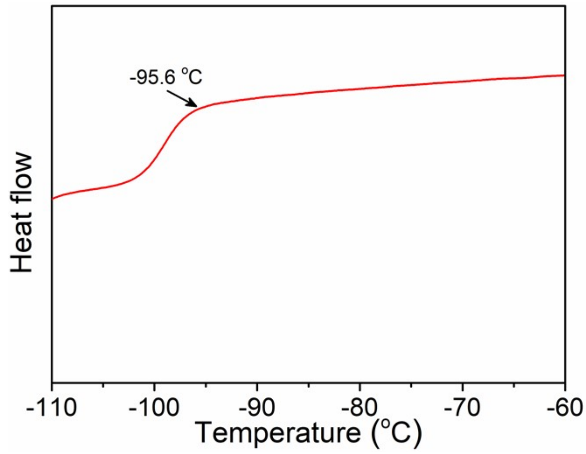

Fig. S4 Dynamic Scanning Calorimetry curve of MDW-20 hydrogels.

Table S1. Comparison of the conductivity and mechanical property of MDW hydrogels and other MXene- or wood-based hydrogels.

Sample	Tensile stress	Compressive stress (MPa)	Conductivity ($S\ m^{-1}$)	Frost resistance (°C)	ref
PAA/Al/Wood hydrogel	2.3	0.6	0.02	/	S1
PVA/AA/Wood hydrogel	15.4	0.48	0.1	/	S2
WA/PIL hydrogel	1.42	1.65	0.23	/	S3
PAA/CNC@TA/MXene	0.14	/	0.12	-20	S4
MCTP hydrogels	0.2	/	2.93	/	S5
PACG-M hydrogel	0.1	2.94	1.3	-20	S6
Cs/PM/MXene hydrogel	0.19	/	0.04	/	S7
MDW hydrogels	0.8	1.44	0.26	-20	This work

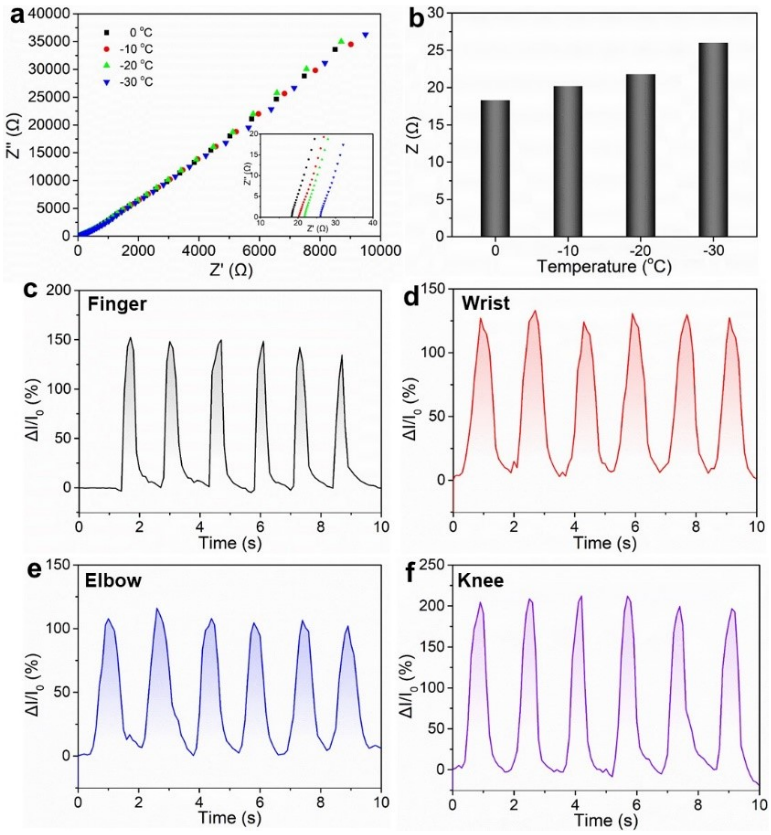

Fig. S5 (a) Nyquist plots and (b) resistance of MDW-20 at low temperatures (0, -10, -20 and -30 °C). Real-time relative electrical current changes of MDW-20 when used as a strain sensor for monitoring various activities including (c) finger, (d) wrist, (e) elbow and (f) knee bending at -20 °C.

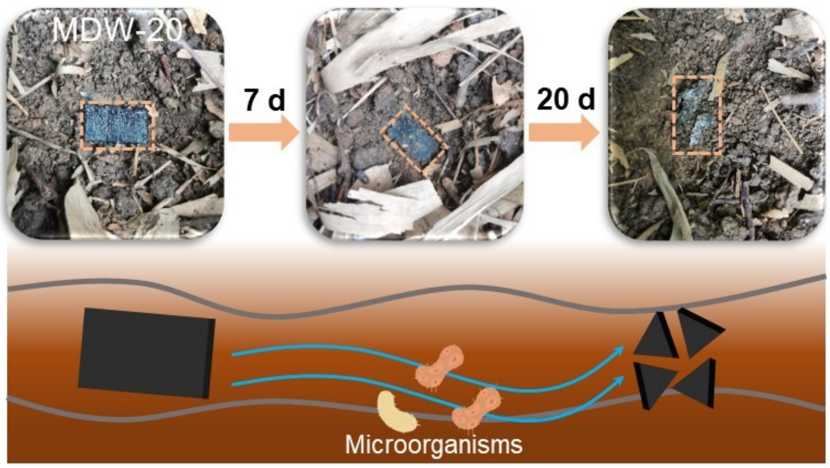

Fig. S6 The Photo of the degradation process.

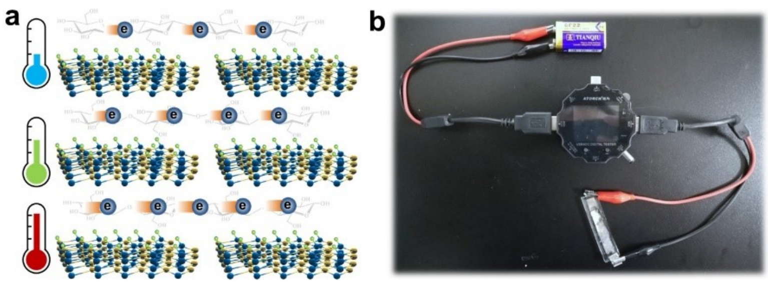

Fig. S7 (a) Temperature sensing mechanism of the MDW-20. (b) Wireless device assembly diagram of the sensor.

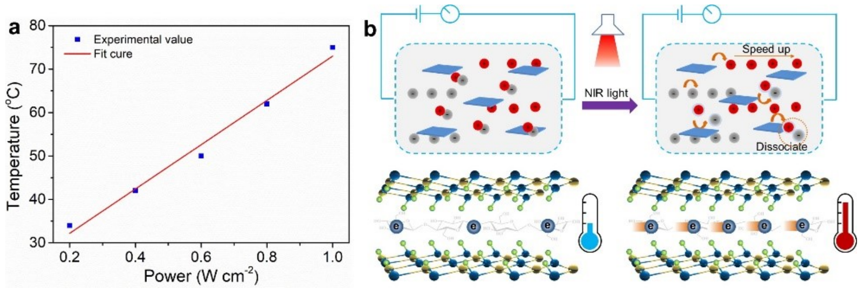

Fig. S8 (a) Experimental data and linear fitting of temperature versus the irradiated power density. (b) Diagram profile of the underlying mechanism for NIR optical sensing.

References

S1. K. Nie, Z. Wang, R. Tang, L. Zheng, C. Li, X. Shen and Q. Sun, *ACS Appl. Mater. Interfaces*, 2020, **12**, 43024-43031.

S2. G. Chen, T. Li, C. Chen, W. Kong, M. Jiao, B. Jiang, Q. Xia, Z. Liang, Y. Liu, S. He and L. Hu, *ACS Nano*, 2021, **15**, 11244-11252.

S3. X. Shen, K. Nie, L. Zheng, Z. Wang, Z. Wang, S. Li, C. Jin and Q. Sun, *J. Mater. Chem. C*, 2020, **8**, 5913-5922.

S4. Y. Lu, X. Qu, S. Wang, Y. Zhao, Y. Ren, W. Zhao, Q. Wang, C. Sun, W. Wang and X. Dong, *Nano Res.*, 2021, **15**, 4421-4430.

S5. P. He, R. Guo, K. Hu, K. Liu, S. Lin, H. Wu, L. Huang, L. Chen and Y. Ni, *Chem. Eng. J.*, 2021, **414**, 128726.

S6. S.-N. Li, Z.-R. Yu, B.-F. Guo, K.-Y. Guo, Y. Li, L.-X. Gong, L. Zhao, J. Bae and L.-C. Tang, *Nano Energy*, 2021, **90**, 106502.

S7. Y. Liu, D. Xu, Y. Ding, X. Lv, T. Huang, B. Yuan, L. Jiang, X. Sun, Y. Yao and J. Tang, *J. Mater. Chem. B*, 2021, **9**, 8862-8870.